Tellus (2003), 55B, 207–214
Printed in UK. All rights reserved

TELLUS
ISSN 0280–6509

Calculating isotopic fractionation from atmospheric measurements at various scales

By JOHN B. MILLER[1,2]* and PIETER P. TANS[1], [1]*Climate Monitoring and Diagnostics Laboratory, National Oceanic and Atmospheric Administration, Boulder, Colorado, USA;* [2]*Institute for Arctic and Alpine Research, University of Colorado, Boulder, Colorado, USA*

(Manuscript received 17 January 2002; in final form 2 September 2002)

ABSTRACT

In this paper we describe some new approaches for calculating isotopic discrimination from atmospheric measurements of CO_2 and $\delta^{13}C$. We introduce a framework that is more flexible than the traditional "Keeling plot" two end-member mixing model, because it allows for the explicit specification of the background values of both CO_2 and $\delta^{13}C$. This approach is necessary for evaluating time series for which one can be certain that the Keeling plot requirement of stable background is violated. We also discuss a robust method for curve fitting and for estimating uncertainty of the fitting parameters. In addition to accounting for the uncertainty associated with measurements, we also account for the uncertainty associated with the appropriateness of the analytical model to the data. Our analysis suggests that uncertainty in calculated source signatures is more strongly related to the appropriateness of the model to the data than to the analytical precision of CO_2 and $\delta^{13}C$ measurements. Relative to our approach, other approaches tend to underestimate the uncertainty in the fitted parameters. There can be substantial uncertainty in slopes and intercepts (two per mil or more) even if R^2 is greater than 0.98. In addition, we note that fitting methods not accounting for uncertainty in both x and y result in systematic biases in the fitted parameters. Finally, we discuss the interpretation of the apparent isotopic source signature when this is a composite of several sources.

1. Introduction

Keeling (1961) introduced a method for relating changes in CO_2 and $\delta^{13}C$ to the isotopic signature of a source or sink adding or removing CO_2 from the background atmospheric CO_2 concentration and isotopic ratio. This technique is used to infer isotopic discrimination by plants during photosynthesis and the isotopic composition of soil and plant respiration (e.g. Yakir and Wang, 1996; Buchmann et al., 1997; Bakwin et al., 1998). By plotting $\delta^{13}C$ vs. the inverse of the CO_2 concentration, the y-intercept is interpreted as the isotopic "signature" of the source or sink. The value of the CO_2 concentration when y equals zero is infinite, so this limit represents the isotopic composition of atmosphere if all the CO_2 in the atmosphere were due to the source. We use the very good approximation (Tans, 1980) that $\delta^{13}\,C \times CO_2$ is conserved, and write the mass balances for atmospheric CO_2 and $\delta^{13}C \times CO_2$ to derive the following:

$$C_{\rm obs} = C_{\rm bg} + C_{\rm s} \tag{1}$$

$$\delta_{\rm obs} C_{\rm obs} = \delta_{\rm bg} C_{\rm bg} + \delta_{\rm s} C_{\rm s} \tag{2}$$

$$\delta_{\rm obs} = \frac{C_{\rm bg}}{C_{\rm obs}}(\delta_{\rm bg} - \delta_{\rm s}) + \delta_{\rm s}. \tag{3}$$

Here, C and δ refer to CO_2 and $\delta^{13}C$, and the subscripts obs, bg and s refer to observed, background and source values. Equation (3) has the linear form $y = m/x + b$, such that $\delta_{\rm s}$ is the y-intercept (b). The great benefit

*Corresponding author.
e-mail: john.b.miller@noaa.gov

of eq. (3) is that the background concentration and delta value of CO_2 can remain unknown. However, the requirement is that they be constant. If desired, that requirement allows for a sensitivity test.

2. A New Model

From eqs. (1) and (2), we can derive a set of new equations that yield new ways of plotting and analyzing data, such that the background values of CO_2 and $\delta^{13}C$ need not be constant. First, we derive an equivalent form of eq. (3), where the background values of CO_2 and $\delta^{13}C$ are unknown.

$$\delta_{obs}C_{obs} = \delta_{bg}C_{bg} + \delta_s(C - C_{bg}) \quad (4)$$

$$\delta_{obs}C_{obs} = \delta_s C_{obs} - C_{bg}(\delta_{bg} - \delta_s). \quad (5)$$

Equation (5) is, like eq. (3), of the linear form $y = mx + b$, except in this case $\delta_s = m$.

To derive the equation in which the background concentration and delta value must be specified, we need only to re-arrange eq. (4):

$$\delta_{obs}C_{obs} - \delta_{bg}C_{bg} = \delta_s(C_{obs} - C_{bg}). \quad (6)$$

The background values used in eq. (6) can take different forms and could be constant or vary with time. Equation (6) is more flexible and explicit than eqs. (3) and (5), but it does require that more information be added.

3. Curve fitting

In order to calculate δ_s as either a slope [eqs. (5) or (6)] or intercept [(eq. (3)] we need to perform a linear regression of our data. The question of how to perform this regression is non-trivial. The typical approach of applying an ordinary least-squares minimization, in which it is assumed that the x-values are not subject to error, results in a systematic bias for the slope and intercept. Not allowing for errors in x always yields a slope or intercept that is smaller in absolute magnitude than if one allows for errors in both x and y. This traditional fit is sometimes referred to as a Model I regression (Sokal and Rohlf, 1995). In contrast, the Model II regression accounts for uncertainty in both x and y. Model II regressions have the property that when the x and y axes are reversed the resulting slope is simply the inverse of the original slope, i.e. the fit is "symmetrical".

There are several fitting techniques that allow for error in x, all of which pass the symmetry test, but yield small differences in the values of fitted parameters. These include "reduced major axis regression", "orthogonal distance regression" and "least-squares bisector" regression. The techniques are summarized and referenced in Table 1. There are small differences in the slopes and intercepts calculated by these techniques, but there does not appear to be consensus as to the preferred Model II technique. Figure 1 shows two examples of atmospheric data fit with both an ordinary least-squares fit and a reduced major axis regression. In panel A, where $R^2 = 0.85$, the Model I regression estimates a slope that is more than 2‰ heavier than the Model II regression. In panel B, where $R^2 = 0.997$, the Model I regression is only 0.2‰ heavier. Here, the difference in the slopes between Model I and Model II is not statistically significant ($P < 0.05$), but the fact that the Model I regression is systematically biased is still cause for concern.

4. Error analysis

Estimating the uncertainty of δ_s as either a slope or intercept is an important part of the curve-fitting process. One choice for parameter error estimation in Model II regressions is to use the uncertainty estimates from a Model I regression (Pataki et al., 2002). Parameter uncertainties may be calculated by formally propagating uncertainties during the linear least-squares fit (Bevington and Robinson, 1992). Here, there is no *a priori* uncertainty associated with the data, and the calculated uncertainty in the parameters is related to the perpendicular distance between the data points and the fitted line. An alternative method is to allow for explicit specification of x and y uncertainties for the data. A starting choice for data uncertainty is the analytical precision of the measurement, which in our case is 0.1 ppm for CO_2 (Conway et al., 1994) and 0.01‰ for $\delta^{13}C$ (Trolier et al., 1996). Knowing the uncertainty in the data, we can test the "goodness of fit" using the chi-square parameter, X^2. From this, we can calculate the chi-square probability, q, which is the probability that an accurate model would give a value for X^2 equal to or greater than that calculated. Values of q close to zero indicate a poor fit between the data and model, quite possibly because of an underestimation of the

Table 1. *Summary of regression techniques*

Regression	Slope	Intercept	Method summary	References
Ordinary Least Squares	−26.632	6893.9	Minimizes the square of the distance in x between data and the fitted line.	
Orthogonal distance; major axis[1]	−26.913	7032.4	Minimizes the square of the normal distances between data points and the fitted line.	York (1966); Boggs et al. (1987)[2]
Geometric mean; reduced major axis[3]	−26.874	7013.1	Slope determined by taking the geometric mean of a normal and 'x, y reversed' Model I regression.	Ricker (1973)
Least-squares bisector	−26.874[4]	7013.1	Sloermined by bisecting the minor angle of a normal and 'x, y reversed' Model I regression.	Sprent and Dolby (1980)

[1]The orthogonal distance and major axis regressions are identical.
[2]This reference describes a weighted orthogonal distance regression.
[3]The slope and intercept derived using the geometric mean regression is equivalent to that of the reduced major axis regression. One of the properties of these regressions is that the slope is equal to the ratio of the standard deviations of the perpendicular x and y distances to the fitted line.
[4]There is a difference between the least-squares bisector and the geometric mean regression, but it is not expressed here (even at 5 significant digits) because of the high correlation in the data.

data uncertainty; values of q near one might indicate an overestimation of the data uncertainty.

In Fig. 1B the calculated value of q is 10^{-9} indicating that the data uncertainty has been underestimated. This could be because analytical errors have been underestimated, or because the model does not ideally represent the sampling conditions, or both. In this case we are fairly certain that our estimates of instrumental uncertainty are accurate. The scatter in the data is more likely due to "natural variability". Each sample was collected at a different time and may have been influenced by different sources or combinations of sources. Thus, we are violating the conditions of our model. Regardless of the causes of the uncertainty, we would like to have error bars on the data that reflect not only instrumental error, but also other kinds of uncertainty, including that associated with the appropriateness of the model for the data. The main reason for wanting to adjust the error bars on the data is that reasonable data uncertainties will yield more realistic slope and intercept uncertainties. Our approach then, is to scale the x and y error bars such that $q = 0.5$. Although this value for q is somewhat arbitrary, other authors refer to fits with $q = 0.5$ as indicative of a "reasonable" fit. (Bevington and Robinson, 1992; Press et al., 1992). This scaling can be performed one of two ways: (1) by iteratively adjusting both the x and y error bars by a single factor until $q = 0.5$, or (2) by scaling the data uncertainty by $[X^2/(N-2)]^{0.5}$ (Bevington and Robinson, 1992). This second approach, which is much simpler computationally, actually yields a reduced X^2 value, $X^2_\nu = 1$, which is equivalent to $q = 0.5$ in the limit of large N. These scaled error bars have no single physical meaning, but are a composite of analytical and sampling errors and deficiencies in the model.

Practically speaking, we calculate our fits by first using a geometric mean regression. Our first estimate of data uncertainty in x and y is the standard deviation of the perpendicular distances between the data points and the fitted line. This ratio of standard deviations in x and y is preserved so that the slope of the line does not change in subsequent steps. Using the routine "fitexy" (Press et al., 1992), we scale the data uncertainties until $q = 0.5$ and then report the uncertainties in the fitted parameters, which are calculated by "fitexy".

Figure 2 shows the effect of the size of x and y error bars on the slope uncertainty using a reduced major axis regression and eq. (5) as our model. Table 2 shows the sensitivity of slope uncertainty to error-bar size for four different data sets. Note that all four data sets have values for R^2 greater than 0.98, but exhibit vastly different slope errors (when $q = 0.5$). R^2 can be a misleading indicator of the uncertainty in the slope or intercept determination. Although none of our

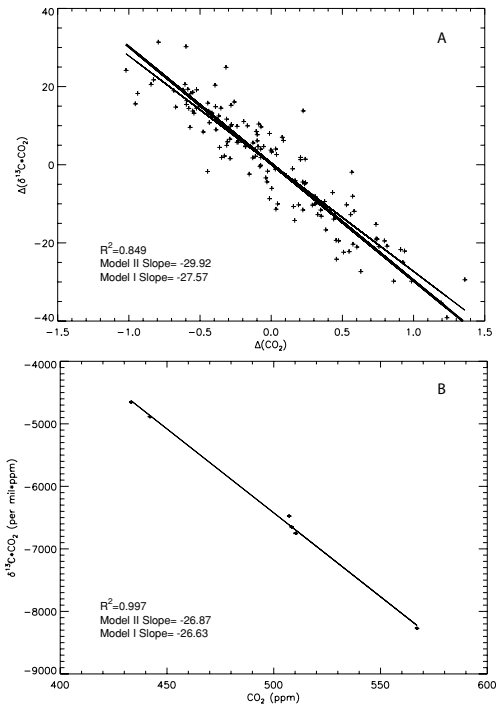

Fig. 1. In panel A, CO_2 and $\delta^{13}C$ data (pluses) from the NOAA/CMDL sampling site in Algeria (ASK) are plotted according to eq. (6), where the "background" values are taken to be the "smooth curve fit" to the data (see text). Fits from both a Model II (reduced major axis; thick line) and Model I (thin line) regression are shown. In panel B, CO_2 and $\delta^{13}C$ from samples collected during night-time in a pine forest adjacent to the NOAA/CMDL sampling station LEF are plotted according to eq. (5). Error bars in B are one sigma uncertainties due to instrumental error; no error bars are shown in A. The bias between Model I and Model II regressions is much larger in A, where R^2 is much smaller than in B.

examples shows this, large values of q may also be a problem, because of the possibility that the data uncertainty has been overestimated. This could lead to an overestimation of the uncertainty of slope and intercept. In most situations in which CO_2 and $\delta^{13}C$ are correlated, however, values of q are low and will lead to an underestimation of slope and intercept uncertainty, when measurement uncertainty is presumed to dominate the data uncertainty. Parameter uncertainties estimated using the 'q' approach are significantly larger than when the measurement uncertainty is used.

However, 'q' uncertainties are only about 10% larger than uncertainties calculated using the ordinary least-squares approach (e.g. Pataki et al., 2002). In the cases we have examined, the 'Model I' approach appears to yield reasonably sized uncertainties. Regardless of the approach, uncertainty in δ_s must be reasonably determined in order to see whether or not relationships exist between δ_s and different environmental or biophysical parameters.

5. Specifying the background values of CO_2 and $\delta^{13}C$

Under what conditions is the stable background assumption implicit in eq. (3) appropriate, and when does it break down in a significant way? Many typical applications of Keeling plots probably come close to satisfying the stable background assumption. These include determining δ_s from a soil respiration chamber and in a stably stratified forest during the night. In both of these examples we have a static atmosphere to which CO_2 is being added in large quantities. At the same time that the data in Fig. 1B were collected, air was sampled 76 m above the forest floor in a nearby location. The CO_2 and $\delta^{13}C$ data from those samples show an increase and decrease, respectively, through the night, indicating a small degree of exchange between the forest canopy and the air above. The CO_2 mole fraction at 76 m changes from 360.7 to 362.3 ppm, and the $\delta^{13}C$ value changes from -7.69 to -7.77‰. We can use these data as our changing background in eq. (6). This results in a value of δ_s indistinguishable from that derived using eq. (5). This happens because δ_s derived for the background itself is about -26‰. If values of CO_2 and $\delta^{13}C$ aloft changed due to advection of air strongly influenced by C_4 vegetation, δ_s of the background would be significantly different. For this hypothetical case, our value of CO_2 changes from 360.7 to 365.5 ppm and $\delta^{13}C$ changes from -7.69 to -7.85‰. The resulting hypothetical value of δ_s for the source to the local forest air would be lighter by only 0.2‰. Because of the large concentration changes near the forest floor, the night-time forest air still satisfies the assumptions of eqs. (3) and (5) reasonably well.

Any time that the background concentration or isotopic ratio of CO_2 is changing over time it is preferable to use eq. (6), if the changes in the background values of CO_2 and $\delta^{13}C$ are known. This is especially true when analyzing a time-series of CO_2 and $\delta^{13}C$ data. Figure 3 shows a record of CO_2 and $\delta^{13}C \times CO_2$ from the NOAA/CMDL Baltic Sea air sampling

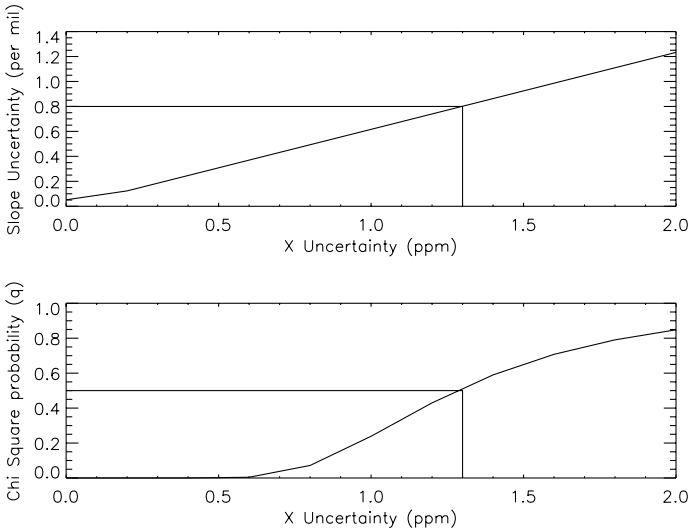

Fig. 2. The bottom panel shows the relationship between the data uncertainty (in x) and the chi-square probability of the fit for the data in Fig. 1B. Because uncertainties in x and y are scaled together (see text), the x uncertainty is always linearly proportional to that in y. The perpendicular lines show the data error associated with $q = 0.5$ (representative of a good fit). The top panel shows the relationship between data uncertainty and the slope uncertainty. For $q = 0.5$, slope uncertainty is about 0.8‰.

Table 2. *Relationship between* X *and slope uncertainty*

	Site	Range (ppm)	X error (ppm)	Slope error (‰)	X error/Slope error	R^2
1	Night-time forest	140	2.32	0.82	2.83	0.9971
1a[1]	Night-time forest	140	0.66	0.23	2.78	0.9998
2	Aircraft	6	0.35	2.02	0.17	0.9819
3	Aircraft	7	0.41	2.37	0.17	0.9857

[1]Data set 1a is identical to 1 with one datum removed.

station (BAL, 55.50°N, 16.67°E). Also shown are the "smooth curve" fits to the data and the long-term trends (Thoninget et al., 1989). In order to determine δ_s here, either as a function of time or as a single value for the entire period, we should take account of the changing backgrounds of CO_2 and $\delta^{13}C$. What values should be chosen to represent C_{bg} and δ_{bg} in eq. (6)?

Our primary application of eq. (6) is in the analysis of long time-series of CO_2 and $\delta^{13}C$ data from the NOAA/CMDL Air Sampling Network (Miller et al., 2002). Here, we have several choices of background values, and this choice determines the meaning of δ_s. One possibility is to choose the long-term (deseasonalized) trend curve as the background values for both CO_2 and $\delta^{13}C$. With this choice we are examining the correlation between CO_2 and $\delta^{13}C \times CO_2$ for the entire seasonal cycle. Although heavily influenced by regional scale biological activity, the seasonal cycle at BAL is also determined by long-range transport of air with high and low values of CO_2 that has been influenced by oceanic CO_2 exchange. In general, the detrended seasonal cycle has a large (mainly zonal) spatial footprint. Thus, our interpretation of δ_s is that it represents a rather large region of the Earth, and accordingly, we must account for the various possible sources contributing to the observed signal.

We might also choose to use the smooth curve fit to the data to represent the background CO_2 and $\delta^{13}C$. Here we are examining the correlation between relatively small differences between the observations and

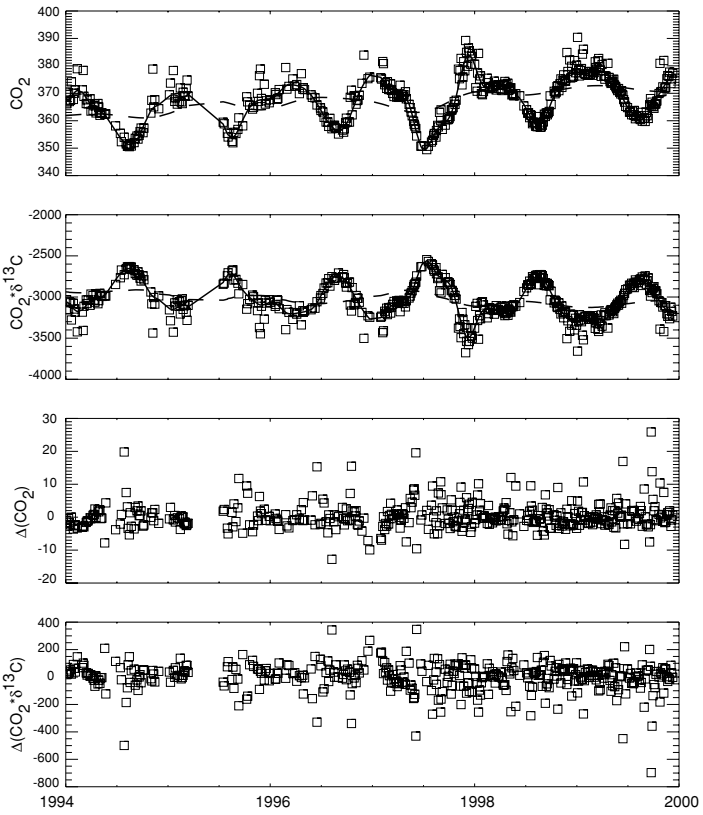

Fig. 3. CO_2 and $\delta^{13}C$ values at NOAA/CMDL Baltic Sea sampling station (BAL). Shown are CO_2 and $\delta^{13}C \times CO_2$ values along with respective smooth curve (solid line) and long-term trend (dashed line) fits to the data. The bottom two panels show residual differences between the smooth curve fits and the data. The slope of the regressions of these residuals is equal to the flux-weighted average isotopic signature of the sources responsible for the variations.

the smooth curve fit. The smooth curve fit is seasonal and as such represents many of the long-range components in the seasonal cycle mentioned above. The differences between the data and the smooth curve will be more strongly influenced by processes occurring on smaller spatial and temporal scales than is the case for the trend curve. For example, the influence of the ocean on the term $(C_{obs} - C_{bg})$ from eq. (6) at a continental site like BAL will be smaller when using the smooth curve to represent the background in eq. (6). Table 3 shows the different values of δ_s with error estimates obtained for these fits. Equation (5) or (6) was used along with the curve fitting and error estimation techniques described above. When δ_s is derived from the raw data without background subtraction, its value is about 2‰ heavier than for the cases where a background is subtracted. Using either the trend or smooth curve to represent the background values of CO_2 and $\delta^{13}C$ is somewhat simplistic. A more sophisticated and accurate approach in applying eq. (6) might involve using values of CO_2 and $\delta^{13}C$ of air some days prior to the air reaching BAL.

Table 3. *Effect of background subtraction on δ_s at BAL*

Method	Model	δ_s (‰)	Uncertainty (%)
Raw data	Eq. (5)	−25.11	0.22
Residual from the trend curve	Eq. (6)	−27.10	0.13
Residual from the smooth curve	Eq. (6)	−26.56	0.21

6. Interpretation of δ_s

δ_s almost never represents the isotopic signature of a single source but rather the flux-weighted average of more than one source and/or sink. Even in the relatively straightforward case of a soil chamber, δ_s might be the flux-weighted average of autotrophic and heterotrophic respiration. We can describe this weighting as follows:

$$\delta_s = \frac{F_a\delta_a + F_b\delta_b}{F_a + F_b}. \quad (7)$$

Here, F represents a flux, and a and b represent different components of the flux with associated isotopic signatures. Equation (7) can be expanded to account for any number of component fluxes. In the case of two kinds of respiration mixing to give δ_s, the interpretation is simple. For example, if autotrophic respiration were 50% of the total flux with a delta value of $-27.0‰$, and δ_s was measured to be $-27.5‰$, this would imply that the signature of heterotrophic respiration was $-28.0‰$.

The decomposition of δ_s becomes counter-intuitive, however, when fluxes of opposing sign are involved. Take, for example, daytime sampling of air above a forest, where the calculated value of δ_s is $-22.0‰$. Say that we estimate the respiration flux to be 5 μmol $m^{-2}\,s^{-1}$ and the assimilation flux to be -20 μmol $m^{-2}\,s^{-1}$. We also have estimated the isotopic signature of the respiration to be $-26.0‰$. Using eq. (7), we can calculate the isotopic signature associated with assimilation, $-23.0‰$. So, the two component isotopic signatures of -26.0 and $-23.0‰$ are combining to yield our measured δ_s of $-22.0‰$! Even small isotopic disequilibria between assimilation and respiration or larger isotopic differences between net biological uptake and fossil-fuel emissions can yield values of δ_s that do not lie between the values of the component fluxes. These counter-intuitive results can occur any time fluxes of opposing sign are combined and then sampled in the atmosphere.

7. Conclusion

We have described a new, general approach for correlating variations in CO_2 and $\delta^{13}C$ that allows for the explicit subtraction of background values for both species. This approach is valuable in situations where the background is not constant through the time or space relevant to the measurements. In instances where the background changes are small relative to the span of the measurements, the traditional "Keeling plot" approach is adequate. However, the commonly used "ordinary least-squares" method of curve fitting is systematically biased, even when values of R^2 are high. The preferable curve fit is a Model II regression, which does not depend on the variable chosen for the x- or y-axis. Another aspect of curve fitting that is important is calculation of uncertainty in the slope and intercept of the lines. We suggest a method that incorporates uncertainties in the collection and analysis of the air samples along with errors associated with the appropriateness of the theoretical model to the data. We feel that without applying this error analysis, uncertainties in the slope and intercept will be underestimated. Finally, we discuss the interpretation of δ_s, which can be decomposed into isotopic signatures associated with constituent fluxes. In cases where all constituent fluxes are of the same sign, the interpretation of the isotopic signatures is intuitive, but when measurements incorporate fluxes of opposing signs, care needs to be taken in the interpretation of δ_s. It should also be noted that both the curve fitting and error analysis issues presented here with respect to CO_2 and $\delta^{13}C$ also apply to other situations where the choice of the x variable is arbitrary and where "natural variability" may be larger than instrumental error; for example, calculating correlations between O_2 and CO_2 and calculating the degree of closure in a surface energy budget.

Our analysis of uncertainty demonstrates that the dominant source of error in the calculation of δ_s, whether by eq. (3), (5) or (6), is not our ability to make careful measurements of CO_2 and $\delta^{13}C$ in the laboratory, but rather the appropriateness of the model to the data. The match between model and data is mostly a function of the atmospheric conditions under which the measurements are made. Improving the precision with which we can calculate δ_s through measurements of CO_2 and $\delta^{13}C$ then depends on choosing our measurement environment to match closely the assumptions in our models.

8. Acknowledgements

John Miller was supported by a National Research Council Postdoctoral Fellowship during this work. We also thank two anonymous reviewers and Matthias Cuntz for suggestions that improved the manuscript.

REFERENCES

Bakwin, P. S., Tans, P. P., White, J. W. C. and Andres, R. J. 1998. Determination of the isotopic (C-13/C-12) discrimination by terrestrial biology from a global network of observations. *Global Biogeochem. Cycles* **12**, 555–562.

Bevington, P. R. and Robinson, D. K. 1992. *Data reduction and error analysis for the physical sciences*, McGraw Hill, Boston.

Boggs, P. T., Byrd, R. H. and Schnabel, R. B. 1987. A stable and efficient algorithm for nonlinear orthogonal distance regression, *SIAM J. Sci. Statist. Comput.* **8**, 1052–1078.

Buchmann, N., Guehl, J. M., Barigah, T. S. and Ehleringer, J. R. 1997. Interseasonal comparison of CO_2 concentrations, isotopic composition, and carbon dynamics in an Amazonian rainforest (French Guiana). *Oecologia* **110**, 120–131.

Conway, T. J., Tans, P. P., Waterman, L. S., Thoning, K. W., Kitzis, D. R., Massarie, K. A. and Zhang, N. 1994. Evidence for interannual variability of the carbon cycle for the National Oceanic and Atmospheric Administration/Climate Monitoring Diagnostics Laboratory Global Air Sampling Network. *J. Geophys. Res.* **99**, 22 831–22 855.

Keeling, C. D. 1961. The concentrations and isotopic abundances of atmospheric carbon dioxide in rural and marine air. *Geochim. Cosmochim. Acta* **24**, 277–298.

Miller, J. B., Tans, P. P., White, J. W. C., Conway, T. J. and Vaughn, B. W. 2002. The atmospheric signal of terrestrial isotopic discrimination and its implication for carbon fluxes. *Tellus* **55B**, this issue.

Pataki, D. E., Ehleringer, J. R., Flanagan, L. B., Yakir, D., Bowling, D., Still, C. J., Buchmann, N., Kaplan, J. O. and Berry, J. A. 2002. The application and interpretation of Keeling plots in terrestrial carbon cycle research. *Global Biogeochem. Cycles* (in press).

Press, W. H., Teukolsky, S. A., Vetterling, W. T. and Flannery, B. P. 1992. *Numerical recipes in C*, Cambridge University Press, New York.

Ricker, 1973. Linear regressions in fishery research. *J. Fish. Res. Board Can.* **30**, 409–434.

Sokal, R. R. and Rohlf, F. J. 1995. *Biometry: the principles and practice of statistics in biological research*, W. H. Freeman and Co., New York.

Sprent and Dolby, 1980. The geometric mean functional relationship. *Biometrics* **36**, 547–550.

Tans, P. P. 1980. On calculating the transfer of carbon-13 in resevoir models of the carbon cycle. *Tellus* **32**, 464–469.

Thoning, K. W., Tans, P. P. and Komhyr, W. D. 1989. Atmospheric carbon dioxide at Mauna Loa Observatory 2. Analysis of the NOAA GMCC data, 1974–1985. *J. Geophys. Res.* **94**, 8549–8565.

Trolier, M., White, J. W. C., Tans, P. P., Massarie, K. A. and Gemery, P. A. 1996. Monitoring the isotopic composition of atmospheric CO_2: Measurements from the NOAA global air sampling network. *J. Geophys. Res.* **101**, 25 897–25 916.

Yakir, D. and Wang, X.-F. 1996. Fluxes of CO_2 and water between terrestrial vegetation and the atmosphere estimated from isotope measurements. *Nature* **380**, 515–517.

York, 1966. Least-squares fitting of a straight line. *Can. J. Phys.* **44**, 1079–1086.